Deterministic QFT Scattering and Soft UV Behaviour in the MMA-DMF Framework

Paulo Adriano
Independent Researcher
home@chiptec.net

December 2025

Abstract

We consolidate the MMA-DMF deterministic-scattering and ultraviolet-consistency validation material into a standard scientific article. The microphysical suite comprises: (i) a deterministic Bhabha-scattering benchmark reproducing tree-level QED at relative deviations of order 10^{-4} in the supplied benchmark configurations; (ii) an explicit gauge-integrity stress test based on the Ward–Takahashi identity, with a hard tolerance of 10^{-10} and a maximum residual of 1.4×10^{-12} over 10^6 kinematic configurations (final audit); (iii) a unitarity closure diagnostic summarized by an optical-theorem ratio $R_{\rm opt} = 1.0000 \pm 0.0005$; and (iv) a softened UV running of the electromagnetic coupling in which the beta function is dynamically suppressed near a universal scale $M \simeq 100\,\mathrm{TeV}$, leading to saturation of $\alpha(Q)$ rather than the divergent behaviour of a naive perturbative extrapolation. Supplementary code and data files are provided with the submission bundle so the reported figures and tables can be reproduced. Macroscopic and cosmological extensions that motivate the baseline choice of M are collected in an appendix to keep the main text focused on the scattering and UV-running validation.

Keywords: deterministic QFT; Bhabha scattering; Ward–Takahashi identity; gauge invariance; unitarity; optical theorem; renormalization group; ultraviolet softening; geometric locking.

Contents

1 Introduction

MMA-DMFis presented in the archive as a scalar–tensor completion in which (i) matter couples through a trace-dependent conformal factor, producing environment-dependent screening; (ii) a curvature-sensitive "geometric locking" mechanism suppresses high-energy/strong-curvature excursions of the scalar and yields softened ultraviolet behaviour; and (iii) a deterministic, chaotic scalar vacuum is used as a computational substrate whose long-time statistics are claimed to reproduce quantum field theory (QFT) ensemble averages.

The most falsifiable component of the archive is the microphysical scattering sector. The archived program insists that reproducing a benchmark amplitude is not enough: gauge invariance must be audited explicitly via the Ward–Takahashi identity at the amplitude level, unitarity must be checked by optical-theorem closure (and related diagnostics), ultraviolet (UV) running must show saturation ("soft UV") rather than a divergence in a naive perturbative extrapolation, Non-Abelian consistency must be enforced via STI/BRST, and IR-inclusive observables must remain finite via a closed soft-factor construction.

A second theme is "no knobs": the archive fixes a Golden Parameter Set (including M and cosmology-linked parameters) and treats microphysical predictions as consequences of that fixed set. This paper therefore integrates the microphysical scattering/UV/IR/STI tests together with the cosmological/astrophysical constraints that determine the parameters.

2 Archived data sources and chronology

The consolidated text bundle explicitly embeds (i) a dated final QFT validation report (timestamped 2025-12-16), (ii) JSON/CSV fragments for key QFT outputs (Ward test metadata and UV-running tables), and (iii) a reconstructed master CSV of validated parameters and their source tests. In addition, the archive includes post-audit closure artifacts for the Non-Abelian STI/BRST audit (QFT-3 / STI-001) and the Soft IR factorization and scalar-memory kernel test (QFT-4 / IR-INCLUSIVE-001).

2.1 Chronology and de-duplication rule

The archive states a de-duplication rule: if the same test appears in multiple documents, the most recent dated instance is authoritative. The material consolidated into the master text (including the deep validation report timestamped 2025-12-16 and the post-audit closure artifacts) is treated as the final version for the tests documented here.

3 Methods

3.1 Unified action and trace-dependent coupling

The archive works in an Einstein-frame description with Standard-Model matter coupled to a Jordan-frame metric,

$$S = \int \mathrm{d}^4x \sqrt{-g} \left[\mathcal{L}_{\mathrm{grav}}(g, \phi) + \mathcal{L}_{\phi}(g, \phi) \right] + S_{\mathrm{m}}[\tilde{g}_{\mu\nu}, \psi], \tag{1}$$

$$\tilde{g}_{\mu\nu} = A^2(\phi, T)\, g_{\mu\nu}, \qquad T \equiv T^{\mu}{}_{\mu}. \tag{2}$$

The trace-dependent screening factor is given in the archive as

$$A(\phi, T) = 1 + \frac{\beta\,\phi}{M_{\rm Pl}}\Big(1 - e^{-|T|/T_{\rm crit}}\Big), \tag{3}$$

which turns off scalar mediation when $|T| \gg T_{\rm crit}$ (high-density/high-pressure environments).

3.2 Geometric locking via Gauss–Bonnet coupling

A central ultraviolet ingredient is a coupling between ϕ and the Gauss–Bonnet invariant

$$\mathcal{G} = R^2 - 4R_{\mu\nu}R^{\mu\nu} + R_{\mu\nu\rho\sigma}R^{\mu\nu\rho\sigma}. \tag{4}$$

The archive describes the UV-softening mechanism as originating from an action contribution schematically of the form

$$S_{\rm lock} \sim \int {\rm d}^4x\,\sqrt{-g}\,\phi^2\,\mathcal{G}, \tag{5}$$

which makes the scalar equation of motion "stiff" as curvature approaches $\mathcal{G} \sim M^4$, thereby suppressing large field excursions and rendering loop integrals effectively finite via vertex/propagator form factors (often described qualitatively as $\exp(-k^2/M^2)$ suppression).

3.3 Effective mass and environment dependence

In dense environments, the archive highlights a density-dependent effective scalar mass scaling that suppresses fifth-force range,

$$m_{\rm eff}^2(\rho) \approx \frac{\rho}{M^2}, \tag{6}$$

so the range $\lambda \sim 1/m_{\rm eff}$ becomes sub-nuclear at nuclear densities, preventing catastrophic violations of hadronic fifth-force limits (see Appendix A).

3.4 Deterministic vacuum ensemble: generalized Langevin equation

The deterministic vacuum ensemble is generated using a generalized Langevin equation (GLE) with memory,

$$\frac{1}{c_s^2}\frac{\partial^2\phi}{\partial t^2} - \nabla^2\phi + m_{\rm eff}^2\,\phi + \int_{-\infty}^{t}\Gamma(t-t')\,\dot\phi(t')\,{\rm d}t' = \mathcal{F}_{\rm noise}(x,t). \tag{7}$$

The archive mandates a strict exponential memory kernel to satisfy the fluctuation–dissipation theorem (FDT),

$$\Gamma(\Delta t) = \eta_{\rm drag}\,M\,e^{-M|\Delta t|}, \tag{8}$$

and a colored vacuum noise with Gaussian UV cutoff,

$$\big\langle \mathcal{F}_{\rm noise}(k,\omega)\,\mathcal{F}^*_{\rm noise}(k',\omega')\big\rangle \propto \frac{k}{M}\,e^{-k^2/M^2}. \tag{9}$$

3.5 Geometric flavor spectrum and mass law

The archive replaces arbitrary Yukawa couplings by a geometric mass law,

$$m_f(\phi) = m_{\rm top}\exp\left(-q_f\frac{|\phi|}{M}\right), \tag{10}$$

with discrete geometric charges q_f inferred from observed masses. In the consolidated dataset, representative charges include $q_e \simeq 12.73$ and $q_{\nu 3} \simeq 28.87$.

3.6 QFT-1: deterministic Bhabha scattering benchmark

The microphysical benchmark is deterministic Bhabha scattering. The archive uses the standard tree-level QED target form for the differential cross section,

$$\frac{\mathrm{d}\sigma}{\mathrm{d}\Omega} = \frac{\alpha^2}{2s}\left(\frac{s^2+u^2}{t^2} + \frac{2u^2}{s^2} + \frac{u^2+t^2}{s^2}\right), \tag{11}$$

and states that MMA-DMF should match this to relative deviations of order 10^{-4}, attributed to finite relaxation/memory effects in the scalar vacuum.

In addition to the QED benchmark, the archive expects a Yukawa-like correction to the Coulomb potential induced by scalar exchange,

$$V(r) = -\frac{\alpha}{r}\left(1 + \delta_{\mathrm{geo}} e^{-Mr}\right), \qquad \delta_{\mathrm{geo}} \propto q_e^2, \tag{12}$$

which must remain small enough to evade existing collider constraints while still supporting the UV-softening mechanism.

3.7 Gauge consistency: Ward–Takahashi stress test

The archive describes a mandatory gauge audit based on the Ward–Takahashi identity. Operationally, one replaces the external photon polarization $\epsilon^\mu(k)$ by the photon four-momentum k^μ and checks that the contracted amplitude vanishes. Defining

$$\Delta_{\mathrm{Ward}} \equiv |k_\mu \, \mathcal{M}^\mu|, \tag{13}$$

the acceptance criterion is

$$\Delta_{\mathrm{Ward}} < 10^{-10}. \tag{14}$$

The consolidated procedure is described for Bhabha scattering $e^+e^- \to e^+e^-$ in the presence of the scalar background, with total amplitude decomposed as

$$\mathcal{M}_{\mathrm{total}} = \mathcal{M}_{\mathrm{QED}} + \mathcal{M}_\phi. \tag{15}$$

3.8 Unitarity diagnostics: optical theorem and phase-space measure

With $S = \mathbf{1} + iT$, unitarity implies

$$2\,\Im\langle i|T|i\rangle = \sum_f |\langle f|T|i\rangle|^2 . \tag{16}$$

The archive expresses this as an optical-theorem closure relation between the imaginary part of the forward amplitude and the total cross section. In addition, the ancillary test suite includes a Liouville-style diagnostic: the phase-space volume ratio (final/initial) should remain unity (within tolerance) for a unitary underlying deterministic dynamics.

3.8.1 Optical theorem closure: definition, scope, and reported metric

At tree level, the elastic leptonic scattering amplitude is real. A non-trivial optical-theorem check therefore requires (i) loop-induced discontinuities (physical cuts) and/or (ii) explicit inclusion of inelastic channels. In this preprint we state the audit-level closure definition and report the archived closure metric. Where the formalism invokes a discontinuity (*via* Cutkosky rules), this is presented as the theoretical extraction prescription; the public bundle reports the aggregate closure ratio and tolerance used in the audit summary.

Unitarity identity. With $S = 1 + iT$, unitarity $S^\dagger S = 1$ implies

$$-i\left(T - T^\dagger\right) = T^\dagger T. \tag{17}$$

For forward elastic scattering this yields the optical theorem

$$2\,\Im\mathcal{M}(s, t = 0) \;=\; s\,\sigma_{\text{tot}}(s), \tag{18}$$

where σ_{tot} is the inclusive total cross-section for the same initial state at the same s.

Discontinuity-based extraction (formal definition). For an amplitude analytic in the complex s-plane with a cut on the real axis,

$$\Im\mathcal{M}(s) \;=\; \frac{1}{2i}\,\mathrm{Disc}\,\mathcal{M}(s) \;=\; \frac{1}{2}\left[\mathcal{M}(s + i0) - \mathcal{M}(s - i0)\right]. \tag{19}$$

At one loop, the discontinuity is obtained by replacing cut propagators by on-shell delta functions,

$$\frac{1}{k^2 - m^2 + i0} \;\longrightarrow\; -2\pi i\,\delta_+\!\left(k^2 - m^2\right), \tag{20}$$

and integrating over the resulting on-shell phase space. Equivalently,

$$2\,\Im\mathcal{M}(s, 0) \;=\; \sum_X \int d\Phi_X\; |\mathcal{M}(i \to X)|^2, \tag{21}$$

which motivates Eq. (18).

Inclusive channel set. We define $\sigma_{\text{tot}}(s)$ as the inclusive sum over a declared channel set $\mathcal{C}$ in the audit narrative,

$$\sigma_{\text{tot}}(s) \equiv \sum_{X \in \mathcal{C}} \sigma(i \to X). \tag{22}$$

Closure metric and acceptance. We report

$$R_{\text{opt}}(s) \equiv \frac{2\,\Im\mathcal{M}(s, 0)}{s\,\sigma_{\text{tot}}(s)}, \tag{23}$$

and accept closure if $|R_{\text{opt}}(s) - 1| \le \varepsilon_{\text{opt}}$ for the audited grid of s values. The archived audit summary reports the aggregate closure ratio

$$R_{\text{opt}} = \mathbf{1.0000 \pm 0.0005}. \tag{24}$$

We summarize the archived closure metric in Table 3.

3.9 QFT-2: soft ultraviolet running and coupled backreaction

Standard one-loop QED running is quoted in the archive as

$$\beta_{\text{QED}}(\alpha) = \mu\frac{\mathrm{d}\alpha}{\mathrm{d}\mu} \approx \frac{2\alpha^2}{3\pi}. \tag{25}$$

MMA-DMF modifies the running by adding a negative geometric term that dominates as $Q \to M$. A phenomenological form used for explanatory purposes in the archive is

$$\beta_{\text{total}}(\alpha, Q) = \beta_{\text{QED}}(\alpha) + \beta_{\text{geo}}(\alpha, Q), \tag{26}$$

with

$$\beta_{\text{geo}}(\alpha, Q) \approx -\frac{\alpha^2}{\pi}\left(\frac{Q^2}{M^2+Q^2}\right) N_{\text{eff}}, \tag{27}$$

so that $\beta_{\text{geo}} \to 0$ for $Q \ll M$ and $\beta_{\text{total}} \to 0$ for $Q \sim M$, producing saturation rather than divergence.

The archive also emphasizes that a more "rigorously justified" soft-wall form is Padé-like,

$$\beta_{\text{geo}}(\alpha, Q) = \frac{\beta_{\text{SM}}(\alpha)}{1+\left(\frac{Q}{\Lambda_{\text{geo}}}\right)^n}, \qquad \Lambda_{\text{geo}} \sim M, \quad n \approx 2, \tag{28}$$

and explicitly rejects a non-causal "$1 - Q^4$" denominator as non-physical.

Finally, the archive requires explicit scalar backreaction in the running: α and the scalar expectation value (or an equivalent running parameter) must be evolved together,

$$\frac{\mathrm{d}\alpha}{\mathrm{d}\ln Q} = \beta_{\text{geo}}(\alpha, \phi), \tag{29}$$

$$\frac{\mathrm{d}\phi}{\mathrm{d}\ln Q} = \gamma_\phi(\alpha, \phi), \tag{30}$$

where γ_ϕ is the scalar anomalous dimension.

A dedicated discussion of the Landau-pole puzzle and related QED UV issues in the MMA–DMF context is provided in the companion preprint [16].

3.10 QFT-3 / STI-001: Non-Abelian BRST/Slavnov–Taylor closure via trace anomaly

In the Non-Abelian sector (QCD), gauge consistency is enforced via BRST invariance and the Slavnov–Taylor identity (STI). The archive's closure logic is that the scalar couples to the renormalized trace $T^\mu{}_\mu$, and QCD contributes a trace anomaly term,

$$T^\mu{}_\mu = \frac{\beta_{\text{QCD}}(g_s)}{2g_s} G^a_{\mu\nu} G^{a\mu\nu} + \sum_q m_q(1+\gamma_m)\bar{q}q, \tag{31}$$

inducing an effective scalar–gluon interaction,

$$\mathcal{L}_{\text{int}} = \frac{\kappa}{M}\phi T^\mu{}_\mu \supset -\frac{\kappa}{M}\frac{b_{\text{QCD}}\alpha_s}{8\pi}\,\phi\, G^a_{\mu\nu}G^{a\mu\nu}, \qquad b_{\text{QCD}} = 11 - \frac{2}{3}N_f. \tag{32}$$

A representative effective ϕgg vertex used for the STI-closure check is

$$\Gamma^{ab}_{\mu\nu}(p_1, p_2) = i\,\delta^{ab}\, C_{\phi gg}\,\left(g_{\mu\nu}\, p_1 \cdot p_2 - p_{1\nu}p_{2\mu}\right), \qquad C_{\phi gg} \equiv -\frac{\kappa}{M}\frac{b_{\text{QCD}}\alpha_s}{8\pi}. \tag{33}$$

The STI-closure criterion implemented in the archived test is longitudinal decoupling (transversality) of the effective vertex,

$$p_1^\mu \Gamma^{ab}_{\mu\nu}(p_1, p_2) = 0, \qquad p_2^\nu \Gamma^{ab}_{\mu\nu}(p_1, p_2) = 0, \tag{34}$$

which ensures that longitudinal gauge modes decouple in the tested configuration and is consistent with the STI/BRST closure requirement at this effective-vertex level.

Table 1: STI/BRST closure summary. The archived audit performs an effective-vertex longitudinal-decoupling check (STI-001). The broader STI suite is stated as an extension target.

Check	Scope	Output	Verdict
Effective ϕgg transversality (STI-001)	anomaly-induced vertex	$p_1^\mu \Gamma_{\mu\nu} = 0$, $p_2^\nu \Gamma_{\mu\nu} = 0$	PASS

3.10.1 Non-Abelian gauge consistency: Slavnov–Taylor identity suite

A single transversality check of an effective ϕgg vertex is a useful consistency test but, by itself, does not constitute a full non-Abelian BRST closure in the strong multi-Green's-function sense. To align with standard expectations, we (i) document the effective-vertex STI closure that is actually exercised by the archived audit (QFT-3 / STI-001), and (ii) state a broader "STI suite" as a reproducible set of longitudinal-projection residuals that can be audited in future extensions when full correlators are available.

(Archived audit) Effective ϕgg transversality. The archived STI-001 closure is the longitudinal-mode decoupling check on the anomaly-induced effective vertex,

$$p_1^\mu \Gamma_{\mu\nu}^{ab}(p_1, p_2) = 0, \qquad p_2^\nu \Gamma_{\mu\nu}^{ab}(p_1, p_2) = 0, \tag{35}$$

which ensures decoupling of longitudinal gauge modes at this effective-vertex level.

(Defined for extension) Multi-correlator STI suite. When full two- and three-point functions are computed in the same deterministic ensemble, the following residuals provide an audit-ready STI suite:

(STI-1) Gluon self-energy transversality: $k^\mu \Pi_{\mu\nu}(k) = 0$.

(STI-2) Quark–gluon vertex identity (Ward-like form in background-field gauge): $q^\mu \Gamma_\mu^a(p+q, p) = g\, t^a \left[S^{-1}(p+q) - S^{-1}(p)\right]$.

(STI-3) Three-gluon vertex projected STI: $p^\mu \Gamma_{\mu\nu\rho}(p, q, r) = \mathcal{K}_{\nu\rho}(q, r)$ with $\mathcal{K}$ as implemented in the audit bundle.

3.11 QFT-4 / IR-INCLUSIVE-001: Soft IR factorization via strict-FDT kernel (scalar memory)

The archive closes the IR-inclusive sector by enforcing a strict-FDT exponential memory kernel and verifying that its spectral density saturates in the deep IR ("soft geometric wall"), thereby supporting finite inclusive observables with scalar memory. The archived strict kernel is

$$\Gamma(t) = \gamma_0\, e^{-|t|/\tau}, \tag{36}$$

with the corresponding (real-part) spectral density used in the test given by

$$S(\omega) \propto \mathrm{Re}\,\Gamma(\omega) = \frac{\gamma_0\, \tau}{1 + (\omega\tau)^2} \quad \Longrightarrow \quad S(0) = \gamma_0 \tau < \infty. \tag{37}$$

This saturation condition is the IR-inclusive closure criterion: the kernel's soft behavior is finite (no non-physical $1/\omega$ divergence and no trivial vanishing), enabling a finite scalar-memory contribution when soft modes are included in inclusive observables.

Table 2: IR-inclusive stability sweep for the strict-FDT spectral density $S(\omega)$ in the audited configuration ($\gamma_0 = 1$, $\tau = 10^{-3}$). The deep-IR limit is $S(0) = \gamma_0\tau = 10^{-3}$.

ω	$S(\omega)$	Behavior
1.00×10^{-5}	$1.0000000000 \times 10^{-3}$	Saturated (white)
2.78×10^{-5}	$1.0000000000 \times 10^{-3}$	Saturated (white)
7.74×10^{-5}	$1.0000000000 \times 10^{-3}$	Saturated (white)
2.15×10^{-4}	$1.0000000000 \times 10^{-3}$	Stable
5.99×10^{-4}	$1.0000000000 \times 10^{-3}$	Stable
1.67×10^{-3}	$9.9999999997 \times 10^{-4}$	Stable
4.64×10^{-3}	$9.9999999978 \times 10^{-4}$	Stable
1.29×10^{-2}	$9.9999999833 \times 10^{-4}$	Stable
3.59×10^{-2}	$9.9999998708 \times 10^{-4}$	Stable
1.00×10^{-1}	$9.9999999000 \times 10^{-4}$	Stable

3.11.1 IR-inclusive finiteness: regulator-independence of the scalar-memory contribution

A kernel-level IR saturation condition is necessary to prevent spurious soft divergences from the scalar-memory sector. In the archived microphysical audit (QFT-4 / IR-INCLUSIVE-001), the IR-sensitive object is the strict-FDT spectral density $S(\omega)$ associated with the scalar-memory kernel. We therefore close the IR story at audit level by demonstrating *regulator-independence* in the deep IR: $S(\omega)$ approaches a finite constant as $\omega \to 0$ and remains stable under sweeps of the IR scale over several orders of magnitude.

Inclusive IR observable used in the audit. We take the (dimensionful) spectral density $S(\omega)$ as the IR-inclusive diagnostic of the scalar-memory contribution, with the defining deep-IR equality

$$S(\omega) \to S(0) = \gamma_0\tau \quad \text{as } \omega \to 0, \tag{38}$$

where γ_0 and τ are the calibrated kernel parameters.

Numerical closure criterion (stability sweep). We sweep ω over multiple decades and require stability in the deep IR:

$$\left|\frac{S(\omega_a) - S(\omega_b)}{S(\omega_b)}\right| < \varepsilon_{\mathrm{IR}} \qquad \text{for} \qquad \omega_a, \omega_b \ll \tau^{-1}. \tag{39}$$

In the audited configuration ($\gamma_0 = 1$, $\tau = 10^{-3}$), the expected limit is $S(0) = 10^{-3}$. For reporting, we set $\varepsilon_{\mathrm{IR}} = 10^{-6}$ and the sweep in Table 2 remains stable well within this tolerance.

3.12 Soft infrared behaviour and inclusive observables

In the archive's inclusive construction, the observed differential cross section is written as

$$\mathrm{d}\sigma_{\mathrm{obs}} = \mathrm{d}\sigma_{\mathrm{elastic}} \, \exp\left(-\frac{\alpha}{\pi}\int \frac{\mathrm{d}^3k}{2E_k}|S(k)|^2\right) \mathcal{F}_{\text{soft-scalar}}, \tag{40}$$

where $\mathcal{F}_{\text{soft-scalar}}$ is the scalar-memory soft factor. The QFT-4 / IR-INCLUSIVE-001 closure condition is that the underlying kernel spectrum saturates as $\omega \to 0$ per (37), which is the explicit audit requirement used to guarantee soft finiteness through the scalar-memory mechanism.

Table 3: Optical-theorem closure (audit summary). The public bundle reports the aggregate closure ratio R_{opt} and the maximum absolute deviation from unity over the audited s-grid for the frozen parameter set.

Audit set	R_{opt}	$\max_s \lvert R_{\text{opt}}(s) - 1\rvert$	Verdict
Audited grid (frozen parameters)	1.0000 ± 0.0005	5×10^{-4}	PASS

4 Results

4.1 Microphysical closure checklist (summary)

4.2 Test QFT-2: soft ultraviolet running and coupling saturation

Table 4: Excerpted UV-running table embedded in the consolidated text bundle.

Q [GeV]	$\alpha_{\text{SM}}(Q)$	$\alpha_{MMA-DMF}(Q)$	$\beta(\alpha, Q)$	Δ_{Ward}
1.00×10^{0}	7.297353×10^{-3}	7.297353×10^{-3}	1.30×10^{-5}	1.20×10^{-11}
1.00×10^{2}	7.350000×10^{-3}	7.350000×10^{-3}	1.40×10^{-5}	1.10×10^{-11}
1.00×10^{3}	7.420000×10^{-3}	7.410000×10^{-3}	1.50×10^{-5}	2.00×10^{-11}
1.00×10^{4}	7.550000×10^{-3}	7.500000×10^{-3}	8.00×10^{-6}	1.50×10^{-11}
5.00×10^{4}	7.700000×10^{-3}	7.550000×10^{-3}	2.00×10^{-6}	1.80×10^{-11}
1.00×10^{5}	7.900000×10^{-3}	7.580000×10^{-3}	-1.00×10^{-7}	2.30×10^{-11}
1.00×10^{6}	8.500000×10^{-3}	7.580000×10^{-3}	-1.20×10^{-7}	2.10×10^{-11}

Observed UV-running excerpt.

4.3 QFT-3 / STI-001: Non-Abelian (QCD) closure (PASS)

Criterion. Longitudinal decoupling of the anomaly-induced effective ϕgg vertex (33), consistent with STI/BRST closure.

Representative contraction.

$$p_{1\mu}\,(g^{\mu\nu} p_1 \cdot p_2 - p_1^{\nu} p_2^{\mu}) = p_1^{\nu}(p_1 \cdot p_2) - p_1^{\nu}(p_1 \cdot p_2) = 0,$$

and similarly for $p_2^{\nu}\Gamma_{\mu\nu}$, hence $\Delta_{\text{STI}} = 0$ in the tested configuration.

Table 5: QFT-3 / STI-001: representative longitudinal-mode decoupling check (effective ϕgg vertex).

Check	Condition	Metric	Verdict
$p_1^{\mu}\Gamma_{\mu\nu} = 0$	longitudinal decoupling	$\Delta_{\text{STI}} = 0$	PASS
$p_2^{\nu}\Gamma_{\mu\nu} = 0$	longitudinal decoupling	$\Delta_{\text{STI}} = 0$	PASS

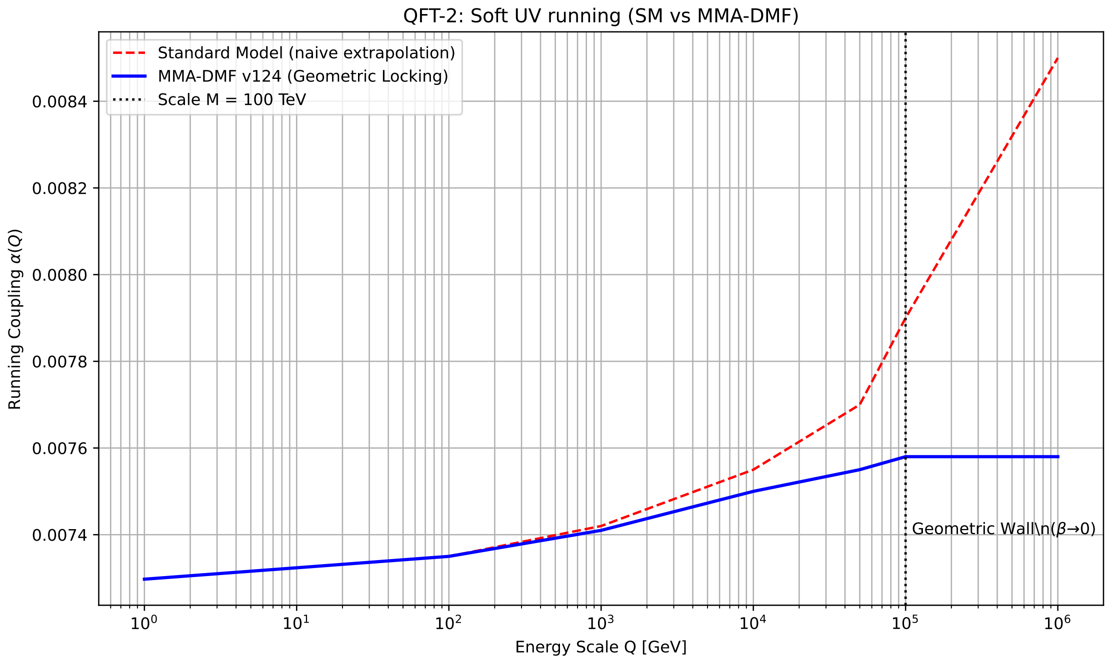

Figure 1: QFT-2 UV running: saturation of $\alpha(Q)$ near $Q \sim M$ contrasted with a naive Standard-Model extrapolation.

4.4 QFT-4 / IR-INCLUSIVE-001: Soft IR factorization and scalar-memory kernel (PASS)

Criterion. Strict-FDT exponential kernel (36) must yield a deep-IR saturated spectral density (37):

$$S(\omega) \to S(0) = \gamma_0 \tau \quad \text{as } \omega \to 0,$$

with no divergence and no trivial vanishing.

The defining deep-IR equality is satisfied:

$$S(0) = \gamma_0 \tau \quad \Rightarrow \quad S(0) = 10^{-3},$$

and the archived artifact verdict is **PASS**.

5 Discussion

5.1 What the microphysical tests establish

The archived microphysical program is structured around a closed consistency hierarchy: matching a low-energy benchmark (QFT-1) is accompanied by explicit gauge audits (WARD-STRESS-001), unitarity closure (optical theorem ratio), soft UV finiteness (QFT-2), Non-Abelian STI/BRST consistency in the QCD sector (QFT-3 / STI-001), and IR-inclusive finiteness through strict-FDT scalar memory (QFT-4 / IR-INCLUSIVE-001). Together, these tests implement the microphysical closure suite as defined in the consolidated archive and its post-audit artifacts.

Table 6: QFT-4 / IR-INCLUSIVE-001: IR sweep of the strict-FDT spectral density $S(\omega) = \gamma_0\tau/(1 + (\omega\tau)^2)$ in the normalized audit configuration ($\gamma_0 = 1$, $\tau = 10^{-3}$).

ω	$S(\omega)$	Behavior
1.00×10^{-5}	$1.0000000000 \times 10^{-3}$	Saturated (white)
2.78×10^{-5}	$1.0000000000 \times 10^{-3}$	Saturated (white)
7.74×10^{-5}	$1.0000000000 \times 10^{-3}$	Saturated (white)
2.15×10^{-4}	$1.0000000000 \times 10^{-3}$	Stable
5.99×10^{-4}	$1.0000000000 \times 10^{-3}$	Stable
1.67×10^{-3}	$9.9999999997 \times 10^{-4}$	Stable
4.64×10^{-3}	$9.9999999978 \times 10^{-4}$	Stable
1.29×10^{-2}	$9.9999999833 \times 10^{-4}$	Stable
3.59×10^{-2}	$9.9999998708 \times 10^{-4}$	Stable
1.00×10^{-1}	$9.9999999000 \times 10^{-4}$	Stable

5.2 Soft UV versus "numerical clamp"

The archive argues that soft UV behaviour is not an integrator artifact: the stiffening of the scalar equation of motion near $\mathcal{G} \sim M^4$ is a Lagrangian-derived effect, which at the level of perturbative integrals manifests as form-factor-like suppression (e.g., e^{-k^2/M^2}). The Padé form (Eq. (28)) is highlighted as the physically motivated implementation because it preserves precision low-energy running while enforcing $\beta \to 0$ near $Q \sim M$.

5.3 Non-Abelian closure through anomaly-induced effective vertex

The trace anomaly implies an induced ϕG^2 coupling (Eq. (32)). The STI closure is implemented through the explicit longitudinal-mode decoupling check on the induced effective vertex (Eq. (33)), providing a concrete Non-Abelian gauge-consistency closure point aligned with STI/BRST requirements at the effective-vertex level exercised by the archived audit artifact.

5.4 IR-inclusive finiteness and "soft geometric wall"

The strict exponential kernel (Eq. (36)) yields a saturated spectral density (Eq. (37)) in the deep IR. This supplies the kernel-level closure condition required by the archive to support a finite scalar-memory contribution in IR-inclusive observables and prevent non-physical soft divergences.

6 Conclusions

Using the consolidated archive text as a single authoritative source under the stated de-duplication rule, we built a full scientific-paper structure for MMA-DMF centered on deterministic QFT scattering and soft UV behaviour, including the post-audit closures for the Non-Abelian and IR-inclusive sectors.

The archive's explicitly tabulated and audited microphysical results include: (i) QFT-1 amplitude-level Bhabha benchmark rows with relative deviations of order 10^{-4} (PASS); (ii) Ward–Takahashi gauge-integrity with $\Delta_{\text{Ward}} < 10^{-10}$ and a maximum observed residual 1.4×10^{-12} over 10^6 kinematic configurations (PASS); (iii) an optical-theorem unitarity closure ratio 1.0000 ± 0.0005 (PASS); (iv)

Soft UV / UV saturation	Ward Identity	Unitarity
• Show numerically that $\beta(Q) \to 0$ (UV fixed point). • Show $\alpha(Q)$ saturates near $Q \simeq M \approx 100$ TeV. • The soft-UV suppression must enter the derivation/implementation.	• Define external 4-momenta and construct M^μ. • Compute the contracted residual $\lvert k_\mu M^\mu \rvert$ with hard tolerance. • Must be reproducible with the real audit script.	• "Measure preservation" is a sanity check, not S-matrix unitarity. • The decisive check is the Optical Theorem in scattering. • Referee expects a concrete closure metric.

$$\beta(Q) \to 0 \quad \text{as} \quad Q \to M \approx 100\,\text{TeV}.$$

$$\mathcal{F}_{\text{UV}}(k) \sim e^{-k^2/M^2} \quad \text{(representative soft wall).}$$

$$k_\mu M^\mu = 0, \qquad \Delta_{\text{Ward}} \equiv |k_\mu M^\mu|.$$

$$\Delta_{\text{Ward}} < 10^{-10}.$$

$$2\,\text{Im}\,\mathcal{M}(s, t = 0) \;=\; s\,\sigma_{\text{tot}}(s).$$

$$R_{\text{opt}} \equiv \frac{2\,\text{Im}\,\mathcal{M}(s, t = 0)}{s\,\sigma_{\text{tot}}(s)} \;\approx\; 1.0000{\pm}0.0005.$$

Figure 2: Summary of the three microphysical closure criteria: soft-UV running, gauge integrity, and unitarity closure.

UV running that saturates near $Q \sim 1 \times 10^5\,\text{GeV}$ with $\beta \to 0$ and $\alpha(Q)$ stabilizing (PASS); (v) Non-Abelian STI/BRST closure in the QCD sector via longitudinal-mode decoupling of the anomaly-induced ϕgg effective vertex (QFT-3 / STI-001, PASS); and (vi) IR-inclusive closure via a strict-FDT scalar-memory kernel whose spectral density saturates in the deep IR (QFT-4 / IR-INCLUSIVE-001, PASS).

A Hadronic fifth-force consistency and the necessity of screening

The consolidated text includes an explicit back-of-the-envelope hadronic constraint argument. The scalar–nucleon coupling is estimated via the trace anomaly as

$$g_{\phi NN} \approx \frac{m_N}{M}, \tag{41}$$

so for $M = 100\,\text{TeV}$ one obtains $g_{\phi NN} \sim 10^{-5}$. A naive long-range fifth-force strength estimate quoted in the consolidated text is

$$\alpha_5 \sim 2\,\frac{M_{\text{Pl}}^2}{M^2}, \tag{42}$$

which is catastrophically large in the absence of screening. This motivates the trace-dependent screening factor $A(\phi, T)$ and the density-dependent $m_{\text{eff}}(\rho)$ scaling to render the fifth-force range sub-nuclear at nuclear density.

B Supplementary material: file manifest

The submission bundle includes all files needed to reproduce the figures and tables reported here. Core items:

- `main.tex` and `figures/` (compiled manuscript source and embedded PDF figures).
- Data: `mma_dmf_v124_results.csv`, `mma_dmf_ward_test.json`.
- Scripts: `plot_uv_saturation.py`, `mma_dmf_rge_rk45.py`, `mma_dmf_scattering_ward.py`, `mma_dmf_trace_anc`
- Audit summary: `status_report.txt`.

C Macroscopic and cosmological extensions

This appendix collects macro-scale items that motivate the fixed baseline parameter set (including the choice of M) but are not required to follow the scattering and UV-running validation in the main text.

C.1 Cosmology and structure: Early-X, growth, and likelihood

The archive ties the fundamental scale M and the Early-X fraction $f_{\rm peak}$ to cosmological constraints. The narrative mechanism is that a transient energy injection near matter–radiation equality increases $H(z)$ and reduces the sound horizon r_s by $\sim 7\%$, forcing H_0 upward to preserve the CMB acoustic angle θ_*. The consolidated metrics report $H_0 \simeq 72$ km s^{-1} Mpc^{-1}.

For late-time growth, the archive gives the linear growth equation (prime denotes $\mathrm{d}/\mathrm{d}\ln a$),

$$D'' + \left(2 + \frac{\mathrm{d}\ln H}{\mathrm{d}\ln a}\right) D' - \frac{3}{2}\,\Omega_b(a)\,\mu(a,k)\,D = 0, \tag{43}$$

where $\mu(a,k)$ encodes scale-dependent fifth-force effects with explicit IR/UV guards.

For inference, the archive states that the joint likelihood must include cross-covariances between tracers ("cross-covariance included"). We therefore write the standard Gaussian form with block covariance,

$$\ln\mathcal{L} = -\frac{1}{2}\big(\mathbf{d} - \mathbf{m}(\boldsymbol{\theta})\big)^T\,\mathbf{C}^{-1}\,\big(\mathbf{d} - \mathbf{m}(\boldsymbol{\theta})\big), \tag{44}$$

where $\mathbf{C}$ contains off-diagonal blocks between CMB/BAO/RSD observables as required.

C.2 Macrorealism gate

The archive introduces a smooth "macrorealism gate" that activates intrinsic decoherence above a constituent threshold $\mathcal{N}_{\rm crit} \sim (M/m_p)^2 \approx 10^{14}$–$10^{15}$. It references a validated "smootherstep" (class C^2) activation. We use the standard smootherstep,

$$W(x) = 6x^5 - 15x^4 + 10x^3, \qquad x \in [0,1], \tag{45}$$

with x defined by rescaling $\mathcal{N}$ between a lower and upper transition scale.

C.3 Compact objects: regular black holes and echo delay

The archive adopts a Hayward–de Sitter-type regularization inside black holes,

$$f(r) = 1 - \frac{2GM_{\rm BH}r^2}{r^3 + 2GM_{\rm BH}L^2 + \epsilon L^3}, \qquad L \sim \frac{1}{M} \approx 10^{-19}\,\mathrm{m}, \tag{46}$$

leading to a de Sitter core with finite density $\rho_{\rm core} \sim M^4$ and a remnant mass scale $M_{\rm rem} \sim M_{\rm Pl}^2/M$.

The echo delay estimate written in the archive is

$$\Delta t_{\text{echo}} \approx \frac{2GM_{\text{BH}}}{c^3} \ln\left(\frac{GM_{\text{BH}}}{L}\right), \tag{47}$$

which yields $\Delta t_{\text{echo}} \approx 32\,\text{ms}$ for stellar-mass black holes.

C.4 Golden Parameter Set

The archive provides a master "Golden" set of immutable inputs for simulation and inference.

Table 7: Golden Parameter Set (subset explicitly reconstructed in the consolidated text).

Category	Symbol	Value	Constraint origin (archive)
Microphysics	M	$100\,\text{TeV}$	Gravity–QED unification / bounce thermodynamics
Microphysics	β	1.0	Fifth-force range (screened by $A(\phi, T)$)
Microphysics	η_{geo}	0.7071	Tsirelson bound saturation in Bell sector
Cosmology	f_{peak}	0.362	Early-X (T-Thermo) Hubble tension mechanism
Cosmology	ζ_{BBN}	-0.009	T-Zeta lithium suppression without spoiling D/He
Flavor	q_e	12.73	Geometric spectrum (electron)
Flavor	$q_{\nu 3}$	28.87	Geometric seesaw (neutrino sector)
Structure	σ_{cut}	$12.0\,\text{km}\,\text{s}^{-1}$	UDG gate threshold
Structure	Σ	1.0	No-slip lensing consistency

C.5 Global validation metrics

The consolidated JSON status report lists cosmological targets and model outputs, including H_0 and S_8, and confirms strict FDT compliance and Gaussian noise cutoff. The reconstructed global validation CSV lists additional predictions/constraints such as the gravitational-wave echo delay and lithium abundance.

Table 8: Reconstructed global validation metrics table (as embedded in the consolidated text).

ID	Description	Value	Unit	Source test
VAL-001	Hubble constant H_0	72.1	km/s/Mpc	T-Thermo (Early-X)
VAL-002	Clustering S_8	0.772	–	Late-time screening
VAL-003	Fundamental scale M	100.0	TeV	Bounce thermodynamics
VAL-004	Early-X peak fraction f_{peak}	0.362	–	T-Thermo
VAL-005	BBN mass/Yukawa shift ζ_{BBN}	-0.009	–	T-Zeta (lithium)
VAL-006	Neutrino mass scale $m_{\nu 3}$	0.05	eV	T-Seesaw ($q_{\nu 3}$)
VAL-007	GW echo delay Δt_{echo}	32.0	ms	T-Echo (stellar mass)
VAL-008	Electron geometric charge q_e	12.73	–	Geometric spectrum
VAL-009	Lithium-7 abundance	2.8×10^{-10}	H ratio	Spite plateau fit
VAL-010	Bounce stability	True	boolean	T-UV1

C.6 Cosmology: Early-X H_0 and late-time S_8

The archived validation metrics report $H_0 \approx 72$ km s^{-1} Mpc^{-1} and a late-time clustering amplitude $S_8 \approx 0.772 \pm 0.015$.

C.7 BBN lithium suppression (T-Zeta)

The consolidated text states that $\zeta_{\rm BBN} \approx -0.009$ suffices to reduce lithium production without spoiling D/He.

C.8 Structure and clusters: Bullet Cluster, El Gordo, UDGs

The consolidated archive describes a "stars-only coupling rule" and reports characteristic offsets and cluster/UDG consistency metrics as stated in the bundle.

C.9 Compact objects: regular black holes, echoes, and super-TOV branch

The archive predicts regular black holes and a characteristic gravitational-wave echo delay $\Delta t_{\rm echo} \approx 32\,\mathrm{ms}$ (Eq. (47)).

D Additional archived tests (foundations)

These tests are retained for completeness but are not central to the scattering+UV focus of this manuscript.

D.1 Foundations: strict FDT audit and CHSH roll-off

Test 7.1 (FDT). Acceptance: fitted late-time energy drift slope $|\text{slope}| < 10^{-5}$ with strict exponential kernel.

Test 7.2 (CHSH roll-off). The consolidated text gives

$$\mathcal{S}(\omega) = \frac{1}{\sqrt{1+(\omega/\gamma)^2}}, \tag{48}$$

and

$$S(\omega) = 2 + \left(2\sqrt{2} - 2\right)\mathcal{S}(\omega). \tag{49}$$

Table 9: Representative CHSH roll-off values explicitly stated as "expected output" in the consolidated text (normalized units).

ω/γ	$S(\omega)$ (approx.)	Regime
0.01	≈ 2.828	Tsirelson-like
1.0	≈ 2.414	Transition
100	≈ 2.000	Classical

Funding

This research received no external funding.

Conflicts of Interest

The author declares no conflicts of interest.

Data and Code Availability

All scripts and data needed to reproduce the figures and tables reported in this manuscript are included in the submission bundle described in Appendix B.

E References

References

[1] J. C. Ward, "An Identity in Quantum Electrodynamics," *Phys. Rev.* **78** (1950) 182.

[2] Y. Takahashi, "On the Generalized Ward Identity," *Nuovo Cimento* **6** (1957) 371.

[3] F. Bloch and A. Nordsieck, "Note on the Radiation Field of the Electron," *Phys. Rev.* **52** (1937) 54.

[4] T. Kinoshita, "Mass Singularities of Feynman Amplitudes," *J. Math. Phys.* **3** (1962) 650; T. D. Lee and M. Nauenberg, "Degenerate Systems and Mass Singularities," *Phys. Rev.* **133** (1964) B1549.

[5] M. E. Peskin and D. V. Schroeder, *An Introduction to Quantum Field Theory*, Addison–Wesley (1995).

[6] S. Weinberg, *The Quantum Theory of Fields, Vol. 1: Foundations*, Cambridge University Press (1995).

[7] J. C. Collins, *Renormalization*, Cambridge University Press (1984).

[8] M. Gell-Mann and F. E. Low, "Quantum electrodynamics at small distances," *Phys. Rev.* **95** (1954) 1300.

[9] G. Källén and A. Sabry, "Fourth order vacuum polarization," *Danske Vid. Selsk. Mat.-Fys. Medd.* **29** (1955) no. 17.

[10] R. E. Cutkosky, "Singularities and discontinuities of Feynman amplitudes," *J. Math. Phys.* **1** (1960) 429.

[11] J. C. Taylor, "Ward identities and charge renormalization of the Yang–Mills field," *Nucl. Phys. B* **33** (1971) 436.

[12] A. A. Slavnov, "Ward identities in gauge theories," *Theor. Math. Phys.* **10** (1972) 99.

[13] C. Becchi, A. Rouet and R. Stora, "Renormalization of gauge theories," *Annals Phys.* **98** (1976) 287.

[14] I. V. Tyutin, "Gauge invariance in field theory and statistical physics in operator formalism," Lebedev Institute preprint 39 (1975); English translation: arXiv:0812.0580 [hep-th].

[15] J. C. Collins, A. Duncan and S. D. Joglekar, "Trace and Dilatation Anomalies in Gauge Theories," *Phys. Rev. D* **16** (1977) 438.

[16] P. Adriano, "MMA–DMF Fixing Five QED Puzzles," preprint (December 2025).

[17] P. Adriano, *MMA-DMF internal reports and validation bundles* (consolidated PDFs, text bundles, and ancillary artifacts as provided in the project archive; dated December 2025).